Multiphysics simulations of the dynamic and wakes of a floating Vertical Axis Wind Turbine

Journal of Physics: Conference Series **1618** (2020) 062053 doi:10.1088/1742-6596/1618/6/062053

Multiphysics simulations of the dynamic and wakes of a floating Vertical Axis Wind Turbine

P Balty, D-G Caprace, J Waucquez, M Coquelet and P Chatelain

Institute of Mechanics, Materials and Civil Engineering, Université catholique de Louvain, 1348 Louvain-la-Neuve, Belgium

E-mail: pierre.balty@uclouvain.be

Abstract. A framework performing Large Eddy Simulations of the flow past Floating Offshore Vertical Axis Wind Turbines (FOVAWT) mounted on semi-submersible platforms is presented. The simulation tool captures the unsteady flow and the resolved 6-DOF motion of the system. A state-of-the-art vortex particle–mesh method solves the aerodynamics and wakes of the turbines. The hydrodynamic loads are accounted for via the relative form of the Morison's equations while the mooring lines tension is computed through a lumped-mass model. Realistic conditions are further obtained by introducing a sheared turbulent inflow and erratic waves in a simulation domain that extends ten diameters downstream of the machine. First, analyses of an isolated FOVAWT wake and motion are performed and the impact of prominent environmental phenomena is assessed. In a second step, the interactions of two FOVAWTs throughout their wakes are studied. In general, the incoming wake signature induces larger oscillation of the downstream machine, alters the shape of the wakes and shortened the transition to turbulence.

1. Introduction

Floating Offshore Vertical Axis Wind Turbines (FOVAWT) have known a growing interest over the last decades. Indeed, offshore turbines are usually subject to stronger and steadier wind compared to onshore machines, promising a higher energy production. Moreover, VAWTs combine the advantages of being insensitive to the wind direction while having a lower centre of gravity. This makes them better suited for floating applications than their horizontal counterpart [1, 2].

These incentives have spurred the development of various projects involving FOVAWTS (DeepCwind, SeaTwirl, S4VAWT, Nenuphar,...) and have led to extensive researches. However, accurate numerical simulations of floating wind turbines require sophisticated aero-hydro-servo-elastic solvers, which often demand a trade-off between accuracy and computational cost [3]. Recent works have studied the aerodynamic performances or the wake of FOVAWT, either using simplified aerodynamic models but fully resolved motions [4, 3, 5], or using basic prescribed motions and CFD [6]. Nevertheless, a comprehensive, high-fidelity study of FOVAWTs in realistic operating conditions has never been proposed.

This work presents the interfacing of a multibody solver with a state-of-the-art CFD method in an innovative framework that enables the Large Eddy Simulation of the flow past H-shaped VAWTs mounted on a semi-submersible platform. The coupled simulations solve the flow together with the 6-degrees of freedom (DOF) motion of the platform under the influence of the rotor loads, the hydrostatic and hydrodynamic loads on the floats, and the mooring

lines. Realistic conditions are obtained by introducing a turbulent inflow with atmospheric shear and by imposing an erratic sea wave profile in a simulation domain that extends ten diameters downstream of the machine. We leverage the potential of this method to identify the prominent environmental factors affecting the motions and wake dynamics of a FOVAWT. We further demonstrate the efficiency of the computational framework in the study of two interacting FOVAWTs and we assess the subsequent effects on the floating dynamics of the waked turbine.

This paper is organised as follows. Section 2 provides a brief description of the developed method and the associated coupling strategies. Section 3 presents the turbine and the platform characteristics, as well as the load cases here considered. FOVAWTs motions, aerodynamics and wakes are then investigated in Section 4. We close this work with conclusions and perspectives in Section 5.

2. Methodology

The VAWT coarse scale aerodynamics and its wake are captured using a Vortex Particle–Mesh (VPM) method. The latter makes the most of two approaches to solve the vorticity-velocity form of the Navier-Stokes equations for incompressible flows: a particle method, characterized by low numerical dissipation and dispersion errors, and a mesh–based approach, enabling the use of highly efficient Poisson solver and finite difference schemes. The generation of vorticity along the blades is accounted for via an immersed lifting line method combined with a dynamic stall model while the turbulent inflow (TI) is synthesised using the Mann algorithm [7]. We refer to [8, 9, 10, 11] (and the references therein) for further details on the VPM method, the immersed lifting lines, and their use in the study of VAWTs.

The hydrodynamic loads exerted on the platform are computed according to the model proposed during the phase II of OC4 project [12]. We choose to only implement the relative form of the Morison's equations. As mentioned in the same reference, this restriction is valid for severe sea states, as those that will be simulated here. The contributions of the main column and of the pontoons are neglected. Irregular waves are generated using a JONSWAP spectrum. The mooring lines are simulated via the lumped-mass model [13]. It shows a better agreement with experimental data than conventional quasi-static solvers but slightly increases the computational load. The torque on the FOVAWT is actively controlled with a maximum power point tracking algorithm [14]. The PI controller optimises the power extraction and partially damps the fluctuations in the torque generator. The power coefficient curve and the controller time constants were computed in a preliminary campaign.

The overall dynamics of the platform are solved in a multi-body solver [15] that gathers the contributions of all the aforementioned effects. At the heart of the simulation tool, this time domain multi-body solver advances the state of the system based on the forces computed by each module. The positions and velocities of the components are then updated and sent back to each subsystem. The process is repeated at every time-step. A typical result of our solver is shown in Fig. 1 and the numerical architecture of the framework is illustrated in Fig. 2.

3. Simulations setup

3.1. Wind turbine and platform characteristics

We simulate an H-type turbine with a diameter of $60\,m$ and a blade height of $96\,m$. The aspect ratio is 1.6. The blades profile is NACA0018 with a chord of $6\,m$. The blade centre is located $72\,m$ above the mean sea level. The VAWT is mounted on top of a DeepCwind semi-submersible platform [12]. This structure has been widely studied in both experiments [16] and simulations [17].

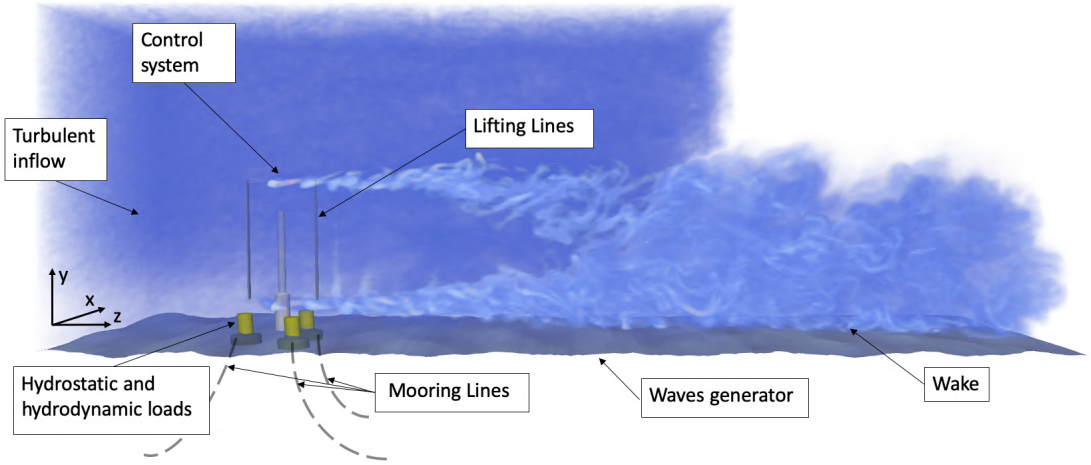

Figure 1: Visualisation of a representative simulation. For the sake of clarity, two distinct color scales have been used for the wake of the VAWT and for the ambient turbulence.

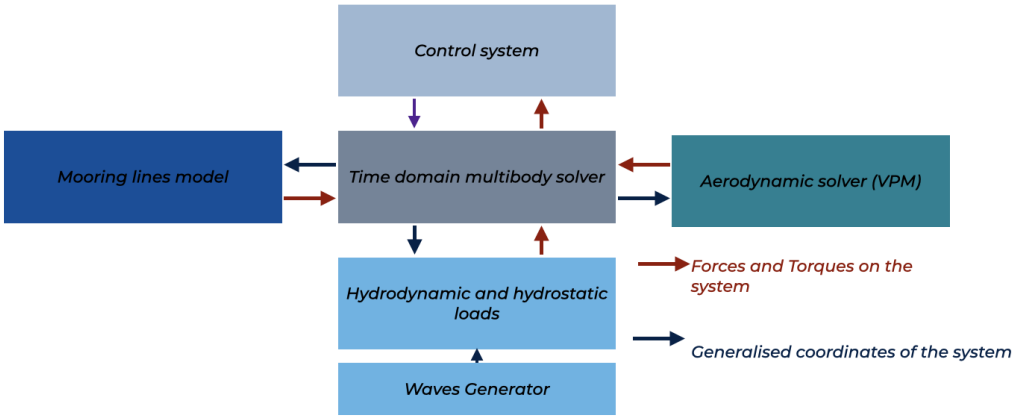

Figure 2: Structure of the implemented framework.

3.2. Load cases

The simulations are all performed with a "blade mid-height" velocity of 15 m/s and a turbulence intensity of about 6 %. The FOVAWT is considered in waves with a significant height of 5.7 m, a period of 10.3 s and a peakness factor $\gamma = 3.3$. The water depth is fixed at 200 m. Four cases are compared and listed in table 1. All four simulations are run over more than 1200 seconds and within a domain of $[4D\text{x}4D\text{x}12D]$ discretized with 6 million particles.

4. Results

4.1. Platform motions

The impact of the flow shear, the turbulence and the wave profile on the turbine mean position is first assessed by performing an analysis of the FOVAWT motion. Figure 3 shows the mean displacements, the standard deviation and the maximum values for every DOF, and for each load case. The turbine response is also decomposed in the frequency domain (Fig. 4).

Comparing all the motions in the time domain (Fig. 3a and 3b), the mean position of the floating device does not deviate markedly from one case to another. Neither the waves nor the

Table 1: Load cases investigated.

Load Case	Waves loads	Wind loads	Number of WT	Turbine separation
LC 1	Periodic waves	Shear	1	—
LC 2	Periodic waves	Shear and TI	1	—
LC 3	Irregular waves	Shear and TI	1	—
LC 4	Irregular waves	Shear and TI	2	$6D$

TI influence the time-averaged position. A closer look at the differences between LC1 and LC2 reveals that the TI induces variations in the surge, sway, pitch and roll motion. Comparing LC2 and LC3 shows that pitch, surge and heave displacements are affected by the wave loading. Finally, motion of the downstream wind turbine diverges from the upstream device, in all DOFs except in the heave direction.

As mentioned in [9], VAWTs produce a net side force; this goes along with a slight deviation of the wake, as it can be seen on the left side of Fig. 9. It also explains the non-zero mean sway and roll. The heave motion, essentially driven by the wave profile, is tightly coupled with the pitch oscillations. The introduction of a TI primarily gives the side force an oscillatory component, inducing variations in the sway position and even more in the roll angle. The spectra (Fig. 4c and 4e) confirms this observation: the turbine response to the turbulence is centred on the natural frequencies of sway and roll. The TI also impacts the surge and the pitch displacements. These DOFs being aligned with the average wind, they are directly correlated with the thrust force on the rotor, which is itself linked to the inflow characteristic. This force induces tension in the mooring lines, which slightly changes the system natural frequency in the surge direction.

The change in wave profile, going from a regular to an erratic spectrum, does not have a significant influence on the system ((Fig. 3a and 3b)). It only alters the standard deviation of the heave and pitch motions. As wind and waves are aligned, and as the platform and the VAWT present a symmetry axis in the wind direction, the insensitivity of the sway and roll to the waves loads is likely specific to our configuration. Regarding the frequency spectrum of the surge (Fig. 4b), we can observe an influence of the waves on displacements in the wind direction.

Finally, differences can be observed by comparing the motion dynamics of two FOVAWTs interacting throughout their wakes. The second device is on average closer to its initial position than the first one. Located in a velocity deficit (see Fig. 9 (d)), it hence experiences a reduced thrust force. The forces in the mooring line are consequently lowered (see table. 2), in particular in their streamwise and spanwise components. The reduced tension may also explain the larger amplitude motion of the system, the DOFs being consequently less stiff. The sway and roll motions are strongly affected; in both cases, their natural frequencies are more excited than for the previous turbines (Fig. 4c and 4e), which induces larger oscillations (Fig. 3).

Table 2: Average forces exerted by the mooring lines on the wind turbines for the two turbines of LC4.

Wind turbine	$F_x\,[kN]$	$F_y\,[kN]$	$F_z\,[kN]$	$\lvert F_{total}\rvert\,[kN]$
Upstream	-74	-2580	-1057	2789
Downstream	-22	-2527	-533	2583

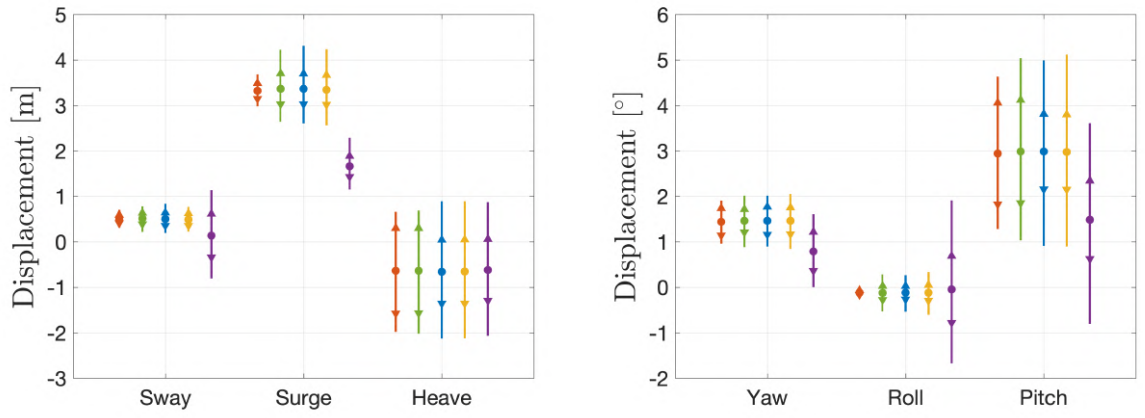

(a) Translations (b) Rotations

Figure 3: Mean displacements of the platform from the nominal position (dot), standard deviation envelope (triangle), range between minimum and maximum values (line). The four cases are considered: LC1 (—), LC2 (—), LC3 (—), LC4 VAWT 1 (—) and LC4 VAWT 2 (—).

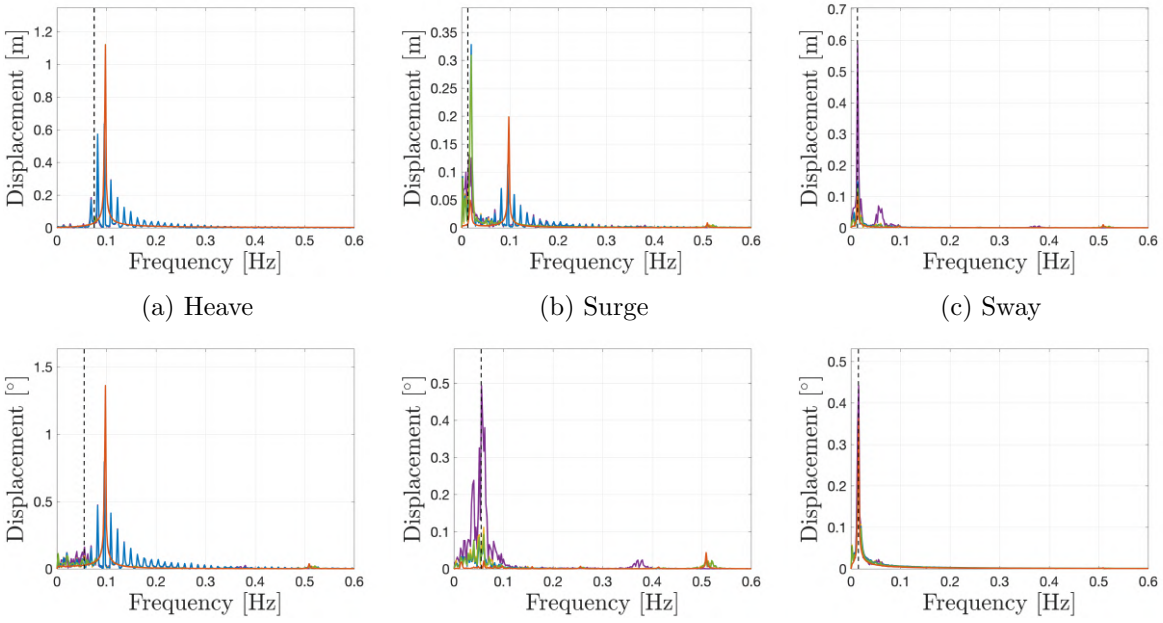

(a) Heave (b) Surge (c) Sway

(d) Pitch (e) Roll (f) Yaw

Figure 4: Motions of the platform in the frequency domain. The four cases are considered: LC1 (—), LC2 (—), LC3 (—), LC4 VAWT 1 (—) and LC4 VAWT 2 (—). Natural frequency of each DOF is illustrated in dashed line (- -).

4.2. Aerodynamics

The previously described motion of the devices certainly affect their aerodynamics. Indeed, any displacement velocity or change in orientation causes a variation in relative velocities as seen by the blades, and the modified angles of attack (AoA) hence affects the performances. In this section, only the first three cases (LC1–3) are considered.

For these scenarios, Fig. 5 illustrates the AoA, and the normal and tangential force coefficients

at mid-blades, respectively $F_n/(cq_0)$ and $F_t/(cq_0)$ — where q_0 is the dynamic pressure of the mean free stream and c is the blade chord. We present the mean evolution of the aforementioned quantities with the azimuth position. The values are averaged over 20 rotor revolutions and standard deviations are given for each situation. We can observe that the main features of those quantities over a blade revolution are conserved. The curves exhibit the expected non-symmetrical behaviour due to the reduced velocity encountered during the downstream leg. In addition, small oscillations are also noticeable in the AoA and force coefficients during the downstream portion, as the blade crosses vortex sheets shed during the upstream leg. As in [10], the standard deviation is the largest when the blade travels perpendicularly to the inflow ($\theta = 90°, 270°$).

The average aerodynamic behaviours are highly similar and the standard deviations are of the same order of magnitude. However, in the first case, their variability is only related to the device motions, while in the other cases, it results from the combined effect of the turbine movements and of the incoming turbulence structures. This induces a slightly wider force coefficients deviation from around 45° to 135°. In general, LC2 deviations are higher than LC3. This is consistent with the standard deviation of the waves, irregular ones owing smaller deviation than the regular ones. The representation of the quantities in the Fourier space (Fig. 6) shows that the most excited frequencies are the Blade Passing Frequency (BPF) and harmonics. As already observed in [18], the difference between the waves and the BPF also appears, at around $0.15\,Hz$ in the three spectra. In the particular case of the tangential force coefficient, the variations due to the TI and waves are of the same order of magnitude than the mean value. They hence appear in the tangential force frequency spectrum. Generally, waves could excite flexible modes of the blades (not simulated here). This must be accounted for during the design of FOVAWTs, to avoid any resonance phenomena.

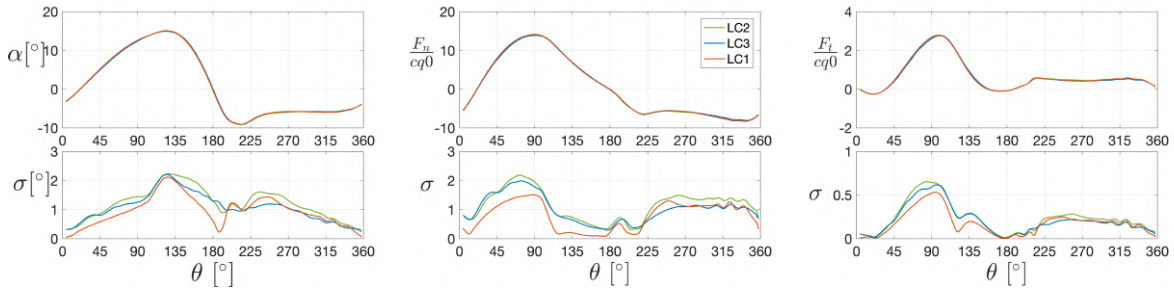

(a) Angle of attack (b) Normal force coefficient (c) Tangential force coefficient

Figure 5: Mean and standard deviations (σ) of the angle of attack and of the normal, $F_n/(cq_0)$, and tangential, $F_t/(cq_0)$, force coefficients at mid-height versus the blade angular position θ for 3 load cases: LC1 (—), LC2 (—), LC3 (—). 20 revolutions are taken into account.

4.3. Wakes

4.3.1. Vortex Dynamics We first study the wakes of one floating device through the visualiation of the instantaneous flow. A volume rendering of the vorticity magnitude $||\boldsymbol{\omega}||$ for LC1 is shown in Fig. 7. It provides a clear insight into the main features of a VAWT wake, which is composed of two types of vortical structures. On the one hand, vortex sheets are shed by the blade because of the time variation of circulation, $d\Gamma/dt$, over a revolution: they form the lateral sides of the wakes. The top and bottom sides of the wake, on the other hand, are composed by tip vortices caused by spanwise variation of circulation. The instabilities of the near-wake region expand further downstream and eventually lead to the merging of vortical structures of various strengths. A more detailed description of the VAWT wake can be found in [9].

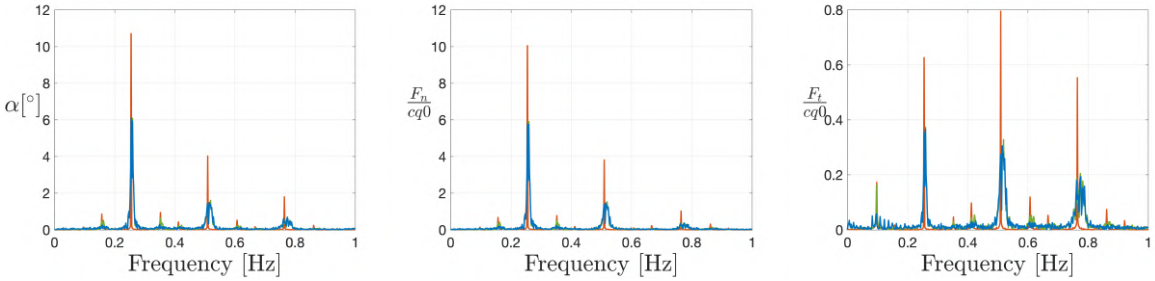

(a) Angle of attack (b) Normal force coefficient (c) Tangential force coefficient

Figure 6: Angle of attack (α), normal and tangential force coefficients ($F_n/(cq_0)$ and $F_t/(cq_0)$) at mid-height in the frequency domain for 3 load cases: LC1 (—), LC2 (—), LC3 (—).

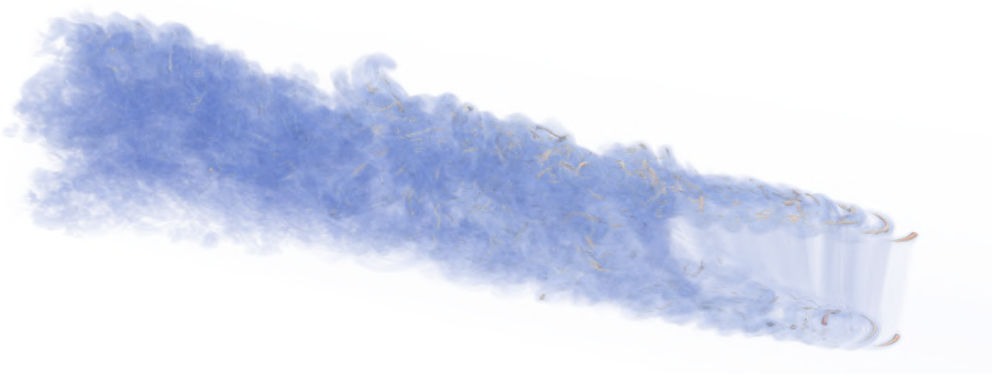

Figure 7: Volume rendering of the vorticity magnitude $||\boldsymbol{\omega}||$ for the load case LC1. Two types of vortical structures compose the wake of a VAWT. The lateral sides of the wake result from vortex sheets originating in the time variation of the circulation around the blades, while the top and the bottom sides consist of tip vortices caused by spanwise variations of circulation.

Figure 8 presents contours of the instantaneous cross-stream vorticity component $(\omega_x, \omega_y)D/U_\infty$ in each load case. Due to heave and pitch displacements, the location of the blade tip changes from one passage to another in the $y-z$ plane. The blade sometimes crosses previously shed tip vortices in the downstream leg (as in Fig.8d, for the second blade of the first wind turbine), and hence generates higher strength vortices; the resulting irregular vortex spacing also eases their pairing or reconnections further downstream. Displacements of the device in the lateral direction increases the time and space irregularity of those events. With an increased number of vortex interactions, the wake of the FOVAWT transitions faster to a fully turbulent state, which should come along with a quicker wake recovery.

On a larger scales, we can observe that the cases with TI exhibit higher wake meandering amplitudes. In the two turbines case (LC4), the amplitude and the period of the s-shaped wake are magnified behind the downstream turbine. This is related to the larger oscillations perpendicular to the freestream (resp. Roll and Surge) that we have underlined in Section 4.1.

4.3.2. Statistics We finally analyse the mean behaviour of the wakes via the time-averaged streamwise velocity field $\bar{u}/U_\infty$ and the time-averaged turbulent kinetic energy TKE/U_∞^2. These statistics were taken over a period of $T_{avg} = 128D/U_\infty$, which corresponds to the flow-through time of the precomputed turbulence. They are shown in Fig 9. The preceding studies [10, 9] have already identified a backflow region in the wakes. This zone coincides with the production

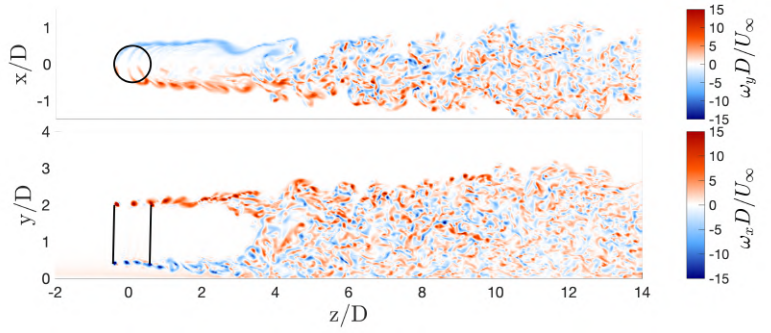

(a) Load case 1

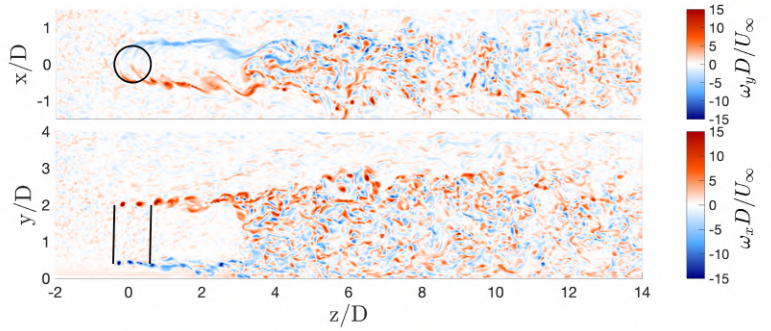

(b) Load case 2

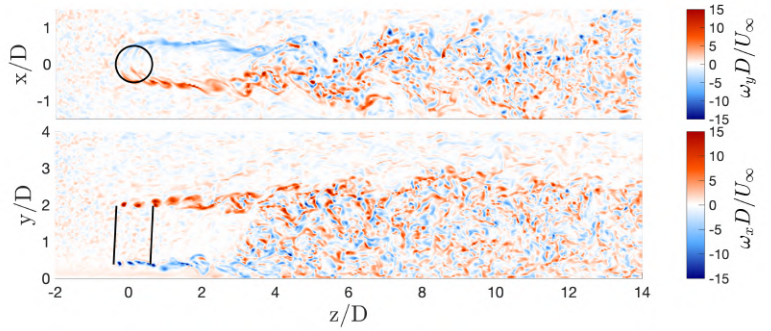

(c) Load case 3

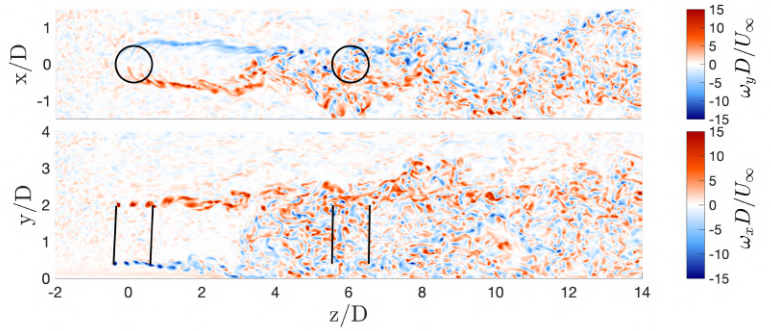

(d) Load case 4

Figure 8: Contours of the instantaneous cross-stream vorticity component $(\omega_x, \omega_y)D/U_\infty$.

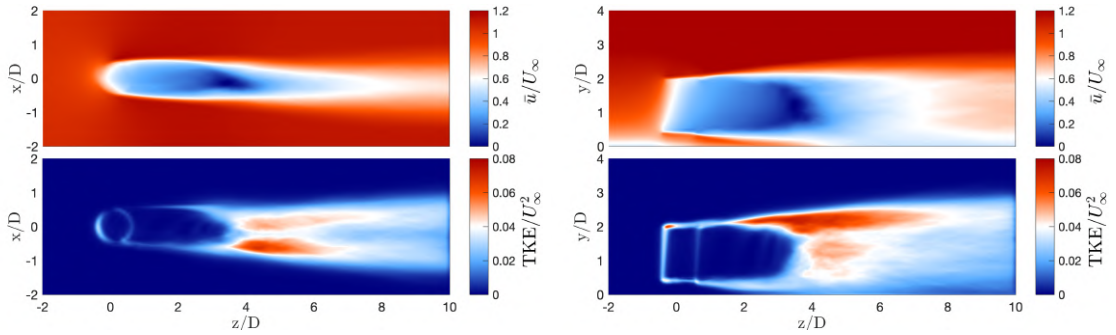

(a) Load case 1

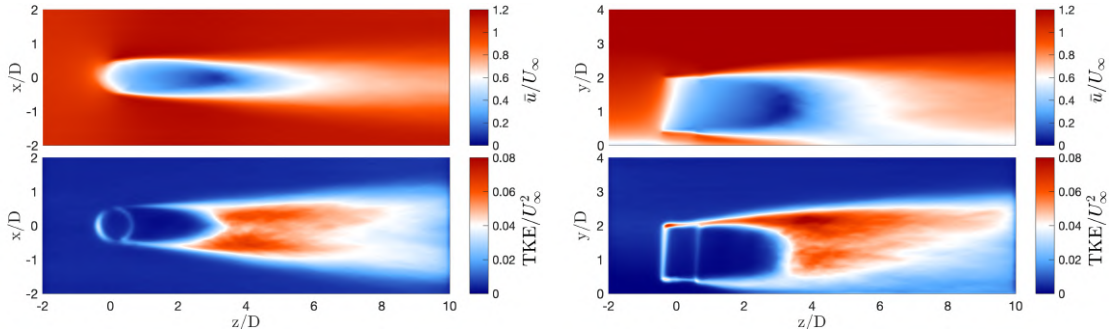

(b) Load case 2

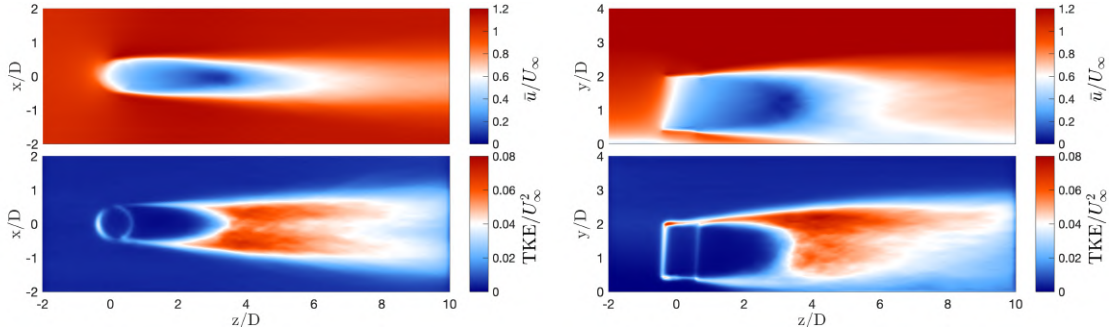

(c) Load case 3

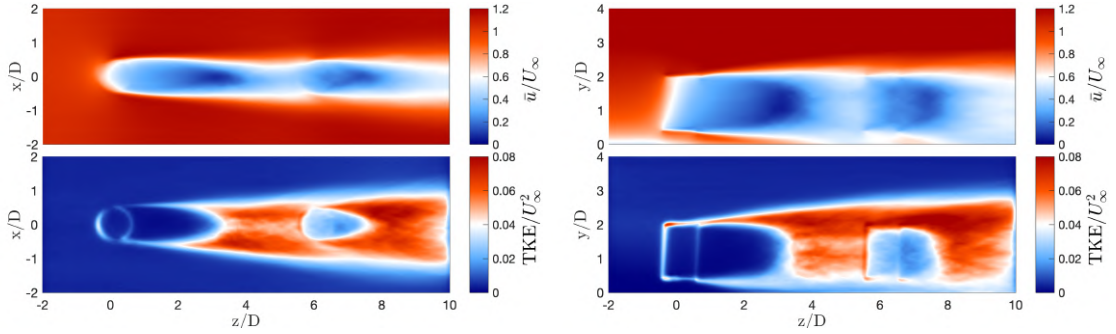

(d) Load case 4

Figure 9: Time-averaged streamwise velocity field $\bar{u}/U_\infty$ and time-averaged turbulent kinetic energy TKE/U_∞^2 at 2/3 of the blades height.

of TKE and an accelerated smearing of the wake velocity deficit. The introduction of TI brings this backflow region closer to the rotor, from around 4D to 3D. The TI combined with greater oscillations in roll, surge and sway also shows a larger area of TKE production. Disordered perturbations in the pitch and heave behaviour (LC3) stimulate the chaotic interactions of the vortices in the y-plane, which on average translates into a more symmetrical topology of the high TKE region. In the x-plane, the TKE production is slightly decreased, at around $y/D = 1$.

In the last case, the backflow region of the downstream wind turbine exhibits a gentler velocity deficit than the one of the upstream device. Furthermore, it is located much closer to the rotor, at around 1D. The region of TKE production is more intense and presents a wider profile. Its topology is constant over the whole width, in contrast to the other cases where the TKE was slightly lower around $x/D = 0$, in the y-plan. It comforts our above discussion: the wake meandering amplitude is higher behind the second turbine, resulting in a more dispersed area of TKE production.

5. Conclusions and perspectives

In this work, we have developed a numerical tool able to simulate the complex dynamics inherent to a floating vertical axis wind turbine mounted on a semi-submersible platform. This tool makes the most of a vortex particle–mesh method combined with a multi-body solver, also gathering the forces due to waves and mooring lines. The VPM method is able to track vortices over long times and distances, which gives a clear insight into the unsteady flow features and dynamics of a floating VAWT, for the first time.

Four cases have been considered. In the first case, the wind turbine was subjected to a sheared inflow and a regular waves loading. The introduction of a turbulent inflow in the system has shown only small impacts on the device motions, but trigger instabilities in the wake, leading to an accelerated transition to a turbulent regime, and a meandering wake signature. A change in the waves loading, going from a regular to an erratic profile has only affected the pitch, surge and heave DOFs of the FOVAWT, but this may be particular to the envisioned configuration where the wind and the waves are aligned. Nonetheless, chaotic waves have resulted in a increase of the vortex interactions leading to a more symmetrical production of turbulent kinetic energy in the wake. Finally, in the last case, a second FOVAWT has been introduced in the wake of the upstream one. It experiences larger amplitude of surge and roll displacements. The wake meandering is consequently enhanced and the velocity deficit zone is strongly reduced.

This constitutes a first insight into the FOVAWT aerodynamics but other factors still need to be addressed. Future works could investigate wind–waves misalignments, other sea states, and their impact on the fatigue of the mooring lines and blades. Moreover, experimental researches are also needed to validate these results.

Acknowledgements

This project has received funding from the European Research Council (ERC) under the European Union's Horizon 2020 research and innovation program (grant agreement no. 725627).
The present research benefited from computational resources made available on the Tier-1 supercomputer of the Fédération Wallonie-Bruxelles, infrastructure funded by the Walloon Region under the grant agreement no.1117545.

References

[1] Borg M and Collu M 2015 *Phil. Trans. R. Soc. A.* **373** 20140076
[2] Cahay M, Luquiau E and Smadja C 2011 Use of a Vertical Wind Turbine in an Offshore Floating Wind Farm *Proc. Offshore Technology Conf.* vol 3
[3] Leroy V, Gilloteaux J c, Combourieu A, Babarit A and Ferrant P 2018 *J. Phys.: Conf. Ser.* **1104** 012001

[4] Cheng Z, Madsen H, Gao Z and Moan T 2017 *Renewable Energy* **107** 604–619
[5] Wang K, Moan T and Hansen M 2016 *Wind Energy* **19** 1853–1870
[6] Lei H, Su J, Bao Y, Chen Y, Han Z and Zhou D 2019 *Energy* **166** 471–489
[7] Mann J 1998 *Probabilistic Engineering Mechanics* **13** 269–282
[8] Chatelain P, Backaert S, Winckelmans G and Kern S 2013 *Flow, Turbulence and Combustion* **91** 587–605
[9] Chatelain P, Duponcheel M, Caprace D G, Marichal Y and Winckelmans G 2017 *Wind Energy Science* **2** 317–328
[10] Chatelain P, Duponcheel M, Zeoli S, Buffin S, Caprace D G, Winckelmans G and Bricteux L 2017 *J. Phys.: Conf. Ser.* **854** 012011
[11] Caprace D G, Winckelmans G and Chatelain P 2020 *Theoretical and Computational Fluid Dynamics* **34** 21–48
[12] Robertson A, Jonkman J, Masciola M, Song H, Goupee A, Coulling A and Luan C 2014 Definition of the Semisubmersible Floating System for Phase II of OC4 Tech. rep. *National Renewable Energy Laboratory*
[13] Hall M and Goupee A 2015 *Ocean Engineering* **104** 590–603
[14] Duponcheel M, Leroi C, Zeoli S, Winckelmans G, Bricteux L, De Jaeger E and Chatelain P 2018 *J. Phys.: Conf. Ser.* **1037** 072046
[15] Caprace D G, Buffin S, Duponcheel M, Chatelain P and Winckelmans G 2017 Large Eddy Simulation of Advancing Rotor for Near to Far Wake Assessment *43rd European Rotorcraft Forum* p 570
[16] Goupee A J, Koo B, Lambrakos K and Kimball R 2012 Model Tests for Three Floating Wind Turbine Concepts *Offshore Technology Conf.* (Houston, Texas, USA)
[17] Robertson A *et al.* 2014 Offshore Code Comparison Collaboration Continuation Within IEA Wind Task 30: Phase II Results Regarding a Floating Semisubmersible Wind System Tech. rep. *National Renewable Energy Laboratory*
[18] Guo Y, Liu L, Gao X and Xu W 2018 *Applied Sciences* **8** 262